Solution Structure of Endothelin-3 Determined Using NMR Spectroscopy†

Robyn G. Mills,‡ Sêan I. O'Donoghue,‡ Ross Smith,§ and Glenn F. King*,‡

Department of Biochemistry, University of Sydney, NSW 2006, Australia, and Department of Biochemistry, University of Queensland, QLD 4072, Australia

Received October 18, 1991; Revised Manuscript Received March 24, 1992

ABSTRACT: The aqueous solution structure of the 21-residue vasoactive peptide hormone endothelin-3 has been determined using high-resolution NMR spectroscopy. A total of 177 proton–proton distance measurements and 5 χ_1 dihedral angle constraints derived from NMR spectra were used to calculate the structure using a combination of distance geometry and dynamical simulated annealing calculations. The calculations reveal a highly ordered, compact conformation in which a helical region extending from K9 to C15 lies in close apposition with the C-terminal hexapeptide; this interaction seems to be largely driven by hydrophobic interactions. Structure–activity studies are interpreted in terms of the conformational features of the calculated endothelin-3 structure.

Endothelin-3 (ET-3)[1] is a member of a family of potent vasoconstrictors, namely, the endothelin (ET) and sarafotoxin (SRTX) peptides. These 21-residue peptides are noted for their strong sequence homology and for evoking remarkably similar biological actions (Kloog & Sokolovsky, 1989; Yanagisawa & Masaki, 1989). The ET/SRTX peptides profoundly affect blood pressure through regulation of the cardiovascular, renal, and neural systems (Vane et al., 1989; Le Monnier de Gouville et al., 1989). Furthermore, endothelin-1 (ET-1) is recognized as the most potent endogenous vasoconstrictor in mammalian vasculature (Randall, 1991).

Although ET-1 and -3 produce a similar spectrum of vascular effects, ET-3 is a less potent vasoconstrictor than ET-1 (Le Monnier de Gouville et al., 1989; Randall, 1991; Inoue et al., 1989), and, unlike ET-1, ET-3 is not expressed in endothelial cells but predominantly in brain, eye, and kidney (MacCumber et al., 1989). The abundance of ET-3 in intestine, brain, and pituitary tissue has led to the proposal that ET-3 may be a new brain–gut peptide (Matsumoto et al., 1989).

ET-3 differs from ET-1 by six variations in the amino acid sequence (Simonson & Dunn, 1990). The three nonconservative substitutions occur in the loop region formed by the disulfide linkage C3–C11; structure–activity studies have indicated that the charged moieties in this loop region are important for activity (Nakajima et al., 1989a). The disulfide bridges C1–C15 and C3–C11, the hydrophobic C-terminal region, and residue W21 also make major contributions to the active conformation of the ET/SRTX peptides (Kimura et al., 1988; Rovero et al., 1990; Nakajima et al., 1989b).

NMR structure studies of ET/SRTX peptides have largely been performed on samples in organic solvents with only a few in aqueous solution. While together they agree on a helical conformation between residues 9 and 15, a consensus has not yet been reached for the C-terminal conformation [e.g., Aumelas et al. (1991), Bortmann et al. (1991), Endo et al. (1989), Krystek et al. (1991), Mills et al. (1991), and Saudek et al. (1989, 1991)].

We have determined the structure of ET-3 in *aqueous* solution. Distance geometry (DG) and dynamical simulated annealing (DSA) calculations were performed using 183 distance and torsion angle constraints derived from ^{1}H NMR experiments. The resulting family of structures, in which the C-terminus adopts a definite preferred conformation, is compared with published structures of ET/SRTX peptides.

Materials and Methods

Materials. Five milligrams of ET-3 (amino acid sequence CTCFTYKDKECVYYCHLDIIW) was purchased from the American Peptide Co. (Santa Clara, CA). 3-Trimethylsilyl[2,2,3,3-^{2}H]propionate (d_4-TSP) was from Fluka A.G. (Buchs, Switzerland). Dr. Peter Güntert kindly provided the DG program, DIANA, and the auxilliary program GLOMSA (Güntert et al., 1991). The molecular dynamics program, X-PLOR, was from Prof. Axel Brünger (Brünger, 1990). Molecular superpositions were performed using the SUPPOS program from the Gröningen BIOMOL protein structure package. The program uses the method of Kabsch (1976) to calculate the rotation for optimal superposition of a pair of structures. All structure calculations and molecular superpositions were performed on a SUN SPARCstation 2GX. Molecular graphics were displayed on a Silicon Graphics IRIS 4D/20 workstation using the MidasPlus software package obtained from the Computer Graphics Laboratory, University of California, San Francisco, CA (Ferrin et al., 1988).

NMR Experiments. ET-3 was dissolved in 95% H_2O/5% D_2O to give a final concentration of 2.22 mM, and 1 mM sodium azide was added. All experiments were performed on the sample at pH 3.6 and 303 K using a Bruker AMX-600 narrow-bore spectrometer with a dedicated proton probe. Chemical shifts were referenced to the methyl resonance of d_4-TSP at 0.00 ppm.

For the measurement of $^3J_{NH\alpha CH}$ coupling constants, a high-resolution one-dimensional NMR spectrum was collected.

† This work was supported by a Grant-in-Aid to G.F.K. and R.S. and a Postgraduate Science Scholarship to R.G.M. from the Australian National Heart Foundation.

* Address correspondence to this author.

‡ University of Sydney.

§ University of Queensland.

[1] Abbreviations: 2D, two dimensional; αCH, α-carbon proton; βCH, β-carbon proton; DG, distance geometry; DQF-COSY, double-quantum filtered correlated spectroscopy; DSA, dynamical simulated annealing; ET, endothelin; FID, free induction decay; FRET, fluorescence resonance-energy transfer; HOHAHA, homonuclear Hartmann–Hahn spectroscopy; NH, amide proton; NMR, nuclear magnetic resonance; NOE, nuclear Overhauser effect; NOESY, nuclear Overhauser effect spectroscopy; RMSD, root-mean-square deviation; d_4-TSP, 3-trimethylsilyl[2,2,3,3-^{2}H]propionate; SRTX, sarafotoxin; τ_m, mixing period in NOESY experiment.

0006-2960/92/0431-5640$03.00/0

The summed FID was double zero-filled, and a Gaussian window function applied. The final digital resolution was 0.1 Hz/pt. Two-dimensional (2D) NMR spectra were recorded in the phase-sensitive mode using time-proportional phase incrementation and a spectral width of 6600 Hz. The sample was not spun for 2D experiments.

The raw data for each 2D experiment consisted of 440–512 FIDs, each consisting of 80–128 scans summed into 4096 complex data points. Generally, prior to Fourier transformation, Gaussian and shifted sine bell window functions were employed in the F_2 and F_1 dimensions, respectively. Following zero-filling in both dimensions, the final transformed data matrix was typically 4096 × 1024 real data points. Baselines were corrected using a third-order polynomial function.

Continuous coherent saturation of the water resonance was performed during the relaxation time (1.5 s) in all experiments, as well in the mixing periods of the NOESY experiments. The spin-lock in 2D HOHAHA experiments, which was obtained using a MLEV-17 isotropic mixing sequence, had a radio-frequency field strength of ~6 kHz.

The buildup of NOESY cross-peak intensity was followed by acquiring NOESY spectra with mixing times ranging from 250 to 450 ms. Those cross peaks which only appeared at the largest mixing times were assessed to result from spin diffusion and were not included in interproton distance calibrations. Proton–proton distance constraints were derived from cross-peak intensities in a 2D NOESY spectrum with τ_m = 350 ms; this NOESY represented a suitable compromise between reasonable cross-peak intensity and minimal spin diffusion effects.

Structure Calculations. Dipolar couplings were classified into four categories of upper distance bounds according to their intensity as judged by contour levels: 2.8 Å (strong), 3.3 Å (medium), 4.0 Å (moderately weak), and 5.0 Å (weak). Lower distance bounds in all calculations were taken to be the sum of the van der Waals radii. In addition, χ_1 torsion angles were constrained to a range of ±30° about the trans position of the αCH and βCH for Val, Ile, and Thr residues with $^3J_{\alpha CH\beta CH}$ > 8 Hz (Wagner et al., 1987; Williamson et al., 1985). The disulfide bridges, C1–C15 and C3–C11, were fixed in all structure calculations by constraining the S–S distance to an upper limit of 2.1 Å and S–βC distances across each bridge to an upper limit of 3.1 Å. Pseudoatoms with appropriate distance corrections were employed for protons which could not be stereospecifically assigned (Wüthrich et al., 1983).

The 251 ^{1}H–^{1}H distance constraints obtained from NOESY cross-peak intensities were filtered through the DG program, DIANA, to eliminate irrelevant constraints (i.e., those distances which are predetermined by the covalent geometry of the molecule or for which no possible conformation will violate the constraint); this yielded a set of 174 structurally important distance constraints. These constraints, along with five χ_1 torsion angle restraints, for residues T2, T5, V12, I19, and I20, were used in initial DG structure calculations.

GLOMSA was then used to extend those stereospecific assignments made directly from the spectra. GLOMSA attempts to make additional stereospecific assignments based on a comparison of initial DG structures with distance constraint lists based on possible stereospecific assignments for a diastereotopic pair of protons (Güntert, 1991). For all GLOMSA analyses, the best 10 structures from the previous DIANA run of 240 calculations were evaluated, and the stereospecific assignments were only accepted if >80% of the structures agreed with the proposed assignment. Iterative use of DIANA and GLOMSA yielded stereospecific assignments for the β-methylene protons of C1 and H16, which increased the number of distance constraints to 177 (44 intraresidue, 77 sequential, and 56 medium to long range). A full list of the 177 distance and 5 dihedral angle constraints used in subsequent DG and DSA calculations can be obtained from the authors upon request.

Finally, DIANA was used to calculate 1000 structures from random starting conformations. The 50 best structures (selected on the basis of their final penalty function values) were then refined in X-PLOR using a modification of the dynamical simulated annealing method described by Clore, Gronenborn, and co-workers (Nilges et al., 1988; Clore & Gronenborn, 1989). Stage 1 of the protocol consists of 50 cycles of energy minimization using the standard X-PLOR parameters for constraining the covalent geometry [k_{bond} = 500 kcal·mol^{-1}·Å^{-2}, k_{angle} = 500 kcal·mol^{-1}·rad^{-2}, $k_{improper}$ = 500 kcal·mol^{-1}·rad^{-2}, and k_{dihed} = 0 kcal·mol^{-1}·rad^{-2}; see Brünger (1990)]. For this stage, nonbonded interactions were modeled by a weak "repel" function which ignores electrical interactions and allows atoms to pass through each other (repel = 1.0 and C_{rep} = 0.002 kcal·mol^{-1}·Å^{-4}). Interatomic distances and χ_1 angles were constrained by experimental energy terms (k_{NOE} = 60 kcal·mol^{-1}·Å^{-2}, asymptote = 0.1, and k_{cdihed} = 50 kcal·mol^{-1}·rad^{-2}). In stage 2, the initial atomic velocities are chosen from a Maxwellian distribution at 1000 K, and the dynamic trajectory is followed for 15 ps in 2-fs steps. During stage 3, the nonbonded repel term (C_{rep}) is increased exponentially (to 0.1 kcal·mol^{-1}·Å^{-4}), and the NOE restraint term (asymptote) is increased linearly (to 1.0) over 9 ps. In stage 4, the system is cooled from 1000 to 300 K (repel = 0.8 and C_{rep} = 4 kcal·mol^{-1}·Å^{-4}) over 2.8 ps. During stage 5, the system is equilibrated at 300 K for 1 ps using Lennard-Jones and Coulomb potentials for nonbonded interactions (repel = 0). This is followed by 1000 cycles of restrained energy minimization (stage 6).

Results

Analysis of DQF-COSY and HOHAHA spectra enabled sequence-specific assignment of the unique E10, V12, and L17 spin systems and residue-specific assignment of resonances arising from T2, T5, K7, K9, I19, and I20. The spin systems of F4 and W21 could be uniquely assigned using intraresidue NOE connectivities between the ring and aliphatic protons observed in NOESY spectra. Having assigned the spin system of F4, sequence-specific assignment of residues 1–6 was determined by sequential NH–NH NOE connectivities from residues 2–6 and sequential αCH–NH and βCH–NH NOE connectivities involving residues 1–4. Prior assignment of the spin systems E10, V12, L17, and W21 and the presence of sequential NH–NH, αCH–NH, and βCH–NH NOEs enabled assignment of the all other residues in the region 10–21. Of the remaining residues, K7, D8, and K9, assignment of D8 was possible as its spin system differs from that of lysines. Although dipolar couplings involving backbone protons of D8 and K9 could not be observed due to the degenerate chemical shifts of the D8 and K9 amide protons, sequence-specific assignment of the lysine residues was possible due to the presence of NOE connectivities between K9 and E10 resonances, and between K7 and D8 resonances. Full chemical shift assignments are listed in Table I; sequential NOEs, used for resonance assignment, are summarized in Figure 1.

Qualitative analysis of the NOE data (see Figure 1) reveals evidence of a helix in the region 9–15, namely, the presence of strong NH–NH connectivities and a large number of medium-range connectivities (i.e., 14 $d_{i,i+3}$ and 4 $d_{i,i+4}$ constraints). Numerous NOE interactions between the helical and C-ter-

Table I: Proton Resonance Assignments of Endothelin-3 at pH 3.6, 303 K[a]

residue	NH	αCH	βCH	β'CH	γCH	γ'CH	γCH_3	$\gamma' CH_3$	δCH	δ'CH	δCH_3	$\delta' CH_3$	εCH
C1		4.42	3.36	3.25									
T2	8.77	4.52	4.07		1.09								
C3	8.34	4.07	3.05	2.62									
T5	7.78	4.36	4.10		1.07								
K7	8.13	4.18	1.80	1.64	1.20				1.62				2.92
D8	8.39	4.60	3.05	2.84									
K9	8.42	4.00	1.87		1.46	1.40			1.65				2.95
E10	8.19	4.35	2.16	2.09	2.50								
C11	8.02	4.26	3.01										
V12	8.01	3.74	1.97				0.86	0.80 (3)[b]					
C15	8.32	4.63	3.20	2.96									
L17	8.01	4.30	1.58	1.53	1.49						0.81		
D18	8.37	4.65	2.87	2.73									
I19	7.78	4.05	1.63		1.26	0.98	0.52				0.70		
I20	7.93	4.13	1.75		1.35	1.06	0.79 (7)[b]				0.75		

residue	NH	αCH	βCH	β'CH	2H	2,6H	3,5H	4H	5H	6H	7H	εNH
F4	8.65	4.57	3.05	2.98		7.22	7.32	7.27				
Y6	8.11	4.55	2.93			7.02	6.76					
Y13	7.77	4.44	2.96			6.93	6.75					
Y14	8.25	4.35	3.05	2.98		7.10	6.80					
H16	8.09	4.54	3.30	3.23	8.51			7.20 (3)[b]				
W21	8.05	4.66	3.33	3.18	7.20 (0)[b]			7.61	7.10	7.17	7.42	10.00

[a] Chemical shifts are referenced internally to the methyl resonance of d_4-TSP at 0.00 ppm. [b] The chemical shifts of the W21-2H, H16-4H, I20 γCH_3, and V12 $\gamma' CH_3$ resonances are given to three decimal places to aid in interpretation of the NOE connectivities in Figure 2.

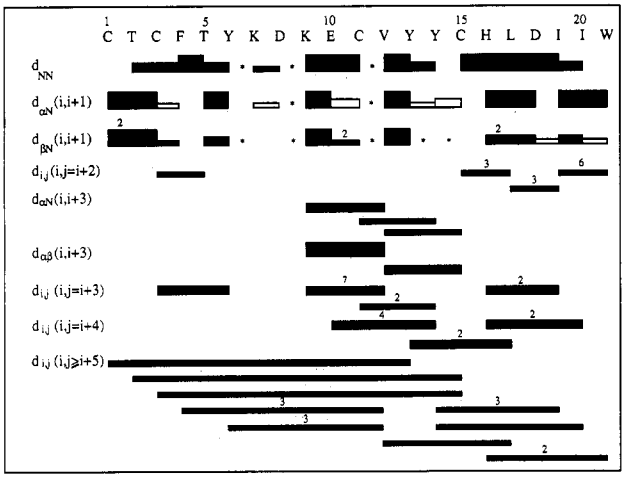

FIGURE 1: Summary of interresidue NOE connectivities observed for ET-3. The solid bars indicate the presence of an NOE and the height of the bar is proportional to the NOE intensity. Open bars indicate NOEs which were irrelevant constraints (and thus eliminated from calculations by DIANA) and asterisks indicate NOEs which could not be unequivocally assigned due to chemical shift degeneracy. Where any particular type of NOE occurs more than once, the number of occurrences is given above the bar. d_{ij} represents an NOE between side-chain protons on residues i and j, with the exception of the NOE observed between the NH of T2 and a βCH of C15.

minal residues were also observed, such as the unequivocal assignment of dipolar couplings between the I19 γCH_3 protons and the ring protons of Y14 (see Figure 2). Such data can only reflect a global fold in the C-terminal region which results in the close association of the C-terminal hexapeptide with residues of the helix.

Following DG/DSA calculations, a family of 30 structures was chosen as best satisfying the NMR-derived constraints; selection was based on the sum of energy penalties due to residual constraint violations. No member of this family has a single distance constraint violation greater than 0.5 Å, and 99.1% of all distance constraint violations are less than 0.3 Å. The structures also display good covalent geometry (mean RMSDs from ideal bond lengths and bond angles are 0.0105 ± 0.0003 Å and 2.503° ± 0.015°, respectively) and good nonbonded contacts (indicated by the negative mean Lennard-Jones potential of −72 ± 5 kcal·mol^{-1}). Figure 3 shows a stereoview of the backbone (N, αC, and C atoms) of this family of ET-3 structures. It can be seen that the NMR-derived constraints tightly define the backbone conformation of residues 9–21: the region 9–15 forms an irregular right-handed helix which is in close apposition to the C-terminal hexapeptide. Convergence in Cartesian space was assessed by comparing the mean RMSDs of the family from the mean structure (obtained by coordinate averaging of the superimposed family of structures). For segments 9–15, 16–21, and 9–21, the mean RMSDs are 0.34 ± 0.13 Å, 0.36 ± 0.12 Å, and 0.71 ± 0.26 Å (calculated for main-chain atoms) and 1.11 ± 0.14 Å, 0.85 ± 0.38 Å, and 1.35 ± 0.39 Å (calculated for all atoms); this compares to mean RMSDs of 0.95 ± 0.24 Å and 1.54 ± 0.37 Å for the main-chain and all atoms of the entire molecule. The quality of superposition reflects the number and distribution of constraints; on average, the conformation of each residue is defined by ~7 constraints in the region 1–8 and by ~10 constraints in the region 9–21. Thus, on average, the calculated conformation corresponds to a second generation NMR structure (Clore & Gronenborn, 1991).

The conformational space occupied by the C-terminal residues 14–21 is well-defined (Figure 4). Figure 5, which shows good superposition of the ϕ and ψ dihedral angles of the best 15 members of the family of structures, is further evidence of the convergence of the calculated structures in this region. The highly ordered side-chain groups adopt a compact conformation as evidenced by numerous short- to medium-range NMR-derived constraints observed for this region. The network of NOE interactions observed between Y14, H16, I19, I20, and W21 results in the aromatic side chains closely fitting around the clustered isoleucyl side chains. This packing is stabilized by hydrophobic forces, with the weakly polar aromatic rings reducing the solvent accessibility of the alkyl groups. As the distance between these aromatic groups (Y14 and W21) is greater than 6.5 Å, it is unlikely that weak polar interactions (Burley & Petsko, 1988) between these groups can contribute to the stability of the C-terminal conformation. The calculated family of structures reveals that the I19 γCH_3 protons lie in close proximity to the indole ring of W21; thus,

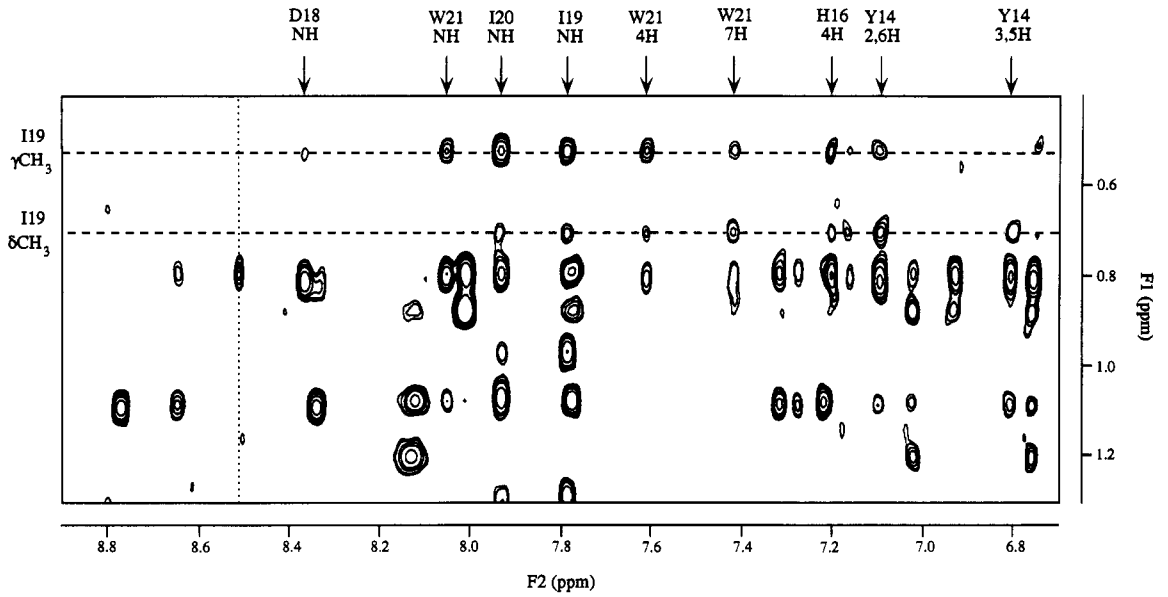

FIGURE 2: Region of the 2D NOESY spectrum (τ_m = 350 ms) of ET-3 (2.22 mM, pH 3.6, 303 K) showing NOE connectivities between proton resonances of the helical and C-terminal residues. The dashed lines highlight dipolar couplings which involve the γ- and δ-methyl groups of I19. The arrows along the F_2 axis indicate the amide and aromatic protons involved in these couplings. The dotted line indicates the position of a strong ridge of "t_1 noise" (Mehlkopf et al., 1984) which results from the intense H16 2H resonance; this ridge is more apparent at higher contour levels and when shifted sine bell rather than Lorentz–Gauss apodization is used in F_2. The apparent cross peak along this t_1 ridge is artifactual.

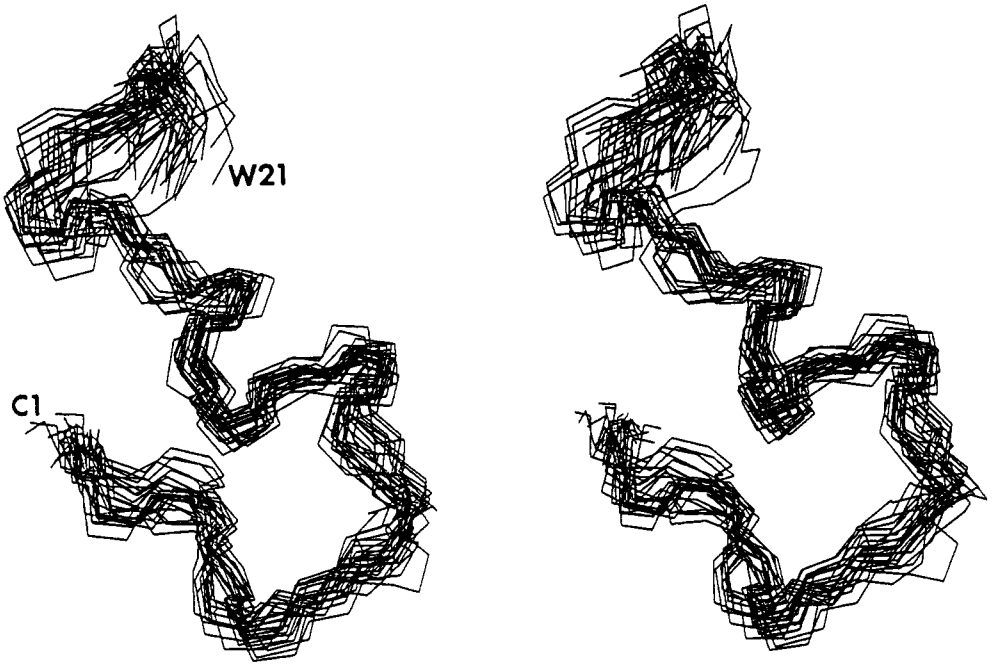

FIGURE 3: Stereoview of the backbones (N, αC, and C atoms) of the family of 30 ET-3 structures obtained from combined DG/DSA calculations. Each member of the family of structures has been superimposed on the mean structure over all residues to give minimum RMSDs between the main-chain atoms (mean structure not shown).

ring current shifts arising from the W21 indole ring appear to be responsible for the dramatic upfield shifting of the I19 γCH_3 resonance.

The loop region formed by the disulfide linkage C3–C11 is the least well defined portion of the family of calculated solution structures, reflecting the lower number of NMR constraints in this region and possibly indicating that it is more conformationally flexible than the rest of the molecule.

Discussion

The family of ET-3 structures calculated in the present study are characterized by an irregular right-handed helix extending from K9 to C15, which is in close apposition with the C-terminus. While the observation of a helical stretch in the region 9–15 is supported by all NMR studies of ET/SRTX peptides so far, only NMR studies published by Saudek et al. (1989, 1991) and Bortmann et al. (1991) and a fluorescence resonance-energy transfer (FRET) study by Pelton (1991) have proposed that the C-terminus adopts a preferred conformation.

The FRET measurements by Pelton (1991) yielded an average intramolecular distance between Y13 and W21 of 12.8 ± 0.6 Å. This is consistent with our results, which give a mean distance of 13.6 Å between the centers of the benzene rings of Y13 and W21. The FRET work of Pelton (1991) also indicates that the W21 indole ring is distal from the disulfides and the imidazole moiety of H16, which concurs with our

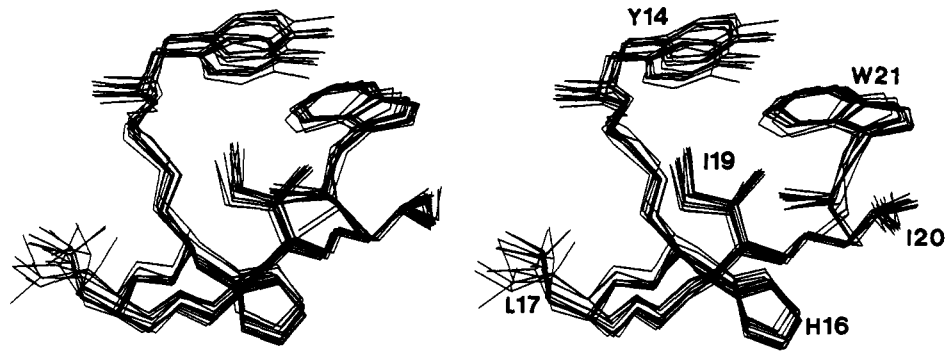

FIGURE 4: Stereoview of the conformation of the C-terminal region (residues 14–21) of ET-3. For clarity, only 13 of the final 30 structures have been shown superimposed over residues 14–21. The carbon backbones of all side chains except those of C15 and D18 have been included to demonstrate the high degree of convergence of the calculated structures.

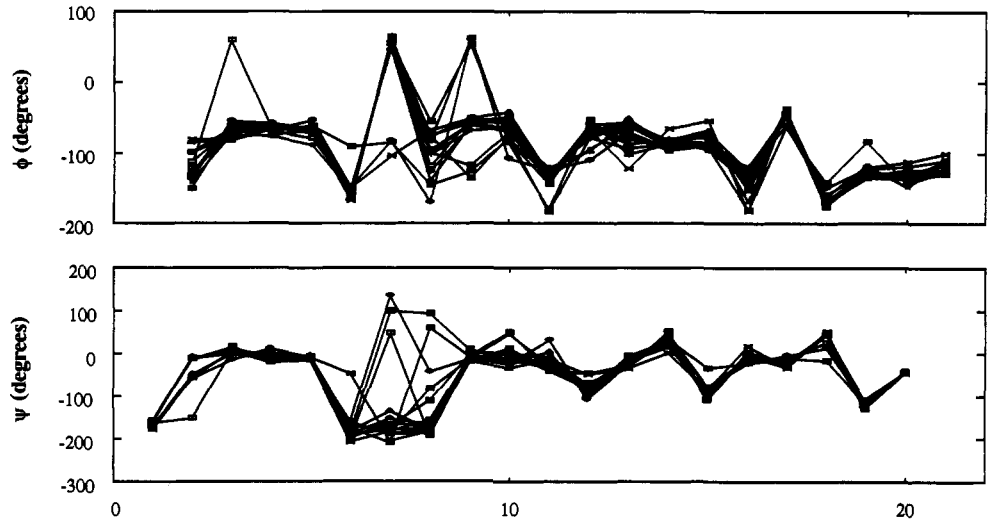

FIGURE 5: Summary of phi (ϕ) and psi (ψ) angles for the best 15 structures. Good convergence is observed for both the ϕ and ψ angles in the region E10–W21 and to a lesser extent in the region C1–T5. The divergence observed for the backbone dihedral angles of residues Y6–K9 reflects the relative paucity of NMR constraints in this region. To avoid separation of the rotamer population spread around ±180°, ϕ and ψ angles between +150° and +180° were expressed using the equivalent negative rotation value (e.g., +150° = −210°).

calculated solution structure. NMR studies of ET-1 in DMSO (Saudek et al., 1991) and ET-3 in 10% acetic acid (Bortmann et al., 1991) have also indicated close association of the C-terminus with the main body of the peptide; however, these authors propose that the C-terminus folds back toward V12–Y13, while in our structure the C-terminus folds back toward the opposite face of the helix, i.e., toward Y14.

However, several NOESY cross-peak assignments which are crucial to the DG calculations of Bortmann et al. (1991) appear to be somewhat tenuous. For example, dipolar connectivities were assigned between the I20 HG1 protons and the aromatic protons of F4. Examination of the relevant portion of the NOESY spectrum and the chemical shift values presented by these authors (Figure 2 and Table II, respectively; Bortmann et al., 1991) reveals that these NOESY cross peaks correlate more closely to a dipolar connectivity between the T5 γCH_3 protons and the aromatic protons of F4, as observed in the present study. Until these tenuous assignments are confirmed, it would be premature to draw comparisons between the structures presented in this study of ET-3 and those of Bortmann et al. (1991).

Our calculated structure enables interpretation of structure–activity studies in terms of the conformational features of the peptide. The hydrophobic clustering of residues 14, 19, 20, and 21, which appears to be the principal force stabilizing the observed C-terminal conformation, is substantiated by structure–activity studies which have shown that all of these residues are important for activity (Hirata et al., 1989; Rovero et al., 1990). For example, studies by Galantino et al. (1991) on the effect of single-point D-amino acid substitutions in ET-1 revealed that substitutions were least tolerated in the C-terminal portion. The binding affinities and contractile activities of analogues which had point substitutions in any of the residues 14–21 were reduced to an average of ~3% and ~1%, respectively, of those characterizing the native peptide. In contrast, residues 5–7, which are not critical for receptor binding or activity (Fleminger et al., 1989; Hirata et al., 1989), are remarkably tolerant to D-amino acid substitutions (Galantino et al., 1991) and appear to be less well constrained than other residues in the calculated solution structure (see, for example, the divergence of the ϕ and ψ angles for this region in Figure 5).

Several studies have targeted the importance of W21 as a critical determinant of endothelin activity. The present work indicates that the indole ring of W21 is involved in stabilization of a hydrophobic C-terminal cluster. Substantial or complete loss of activity due to the removal or addition of amino acids at the C-terminus (Hirata et al., 1989; Nakajima et al., 1989a) may be a consequence of substantial disruption of the highly ordered core of hydrophobic residues in this region. Replacement of W21 with other aromatic L-amino acids, such as Phe or Tyr, probably enables maintenance of those hy-

drophobic interactions which stabilize the C-terminal cluster of nonpolar residues, thus explaining the observed moderate reduction in biological activity for these substitutions (Nakajima et al., 1989b).

We recently determined the conformation of SRTX-6b in water (Mills et al., 1991), the first structure determination of an ET/SRTX peptide in native solvent. This study also yielded several turns of helix (from K9 to H16), but no preferred conformation for the C-terminal hexapeptide segment of SRTX-6b. However, short-range dipolar interactions between residues 19, 20, and 21 were noted, and the upfield shifting of one of the V19 γCH_3 resonances was proposed to result from ring-current shifting caused by proximity to W21. Thus, the hydrophobic association of residues 19 and 21, as observed in the current study for ET-3, seems to be a common feature of the ET/SRTX peptides, even if it remains unclear whether the C-terminus of the SRTX peptides is closely associated with the main body of the peptide in aqueous solution (Mills et al., 1991).

In summary, the present study has shown that endothelin-3 in aqueous solution adopts a highly ordered, compact conformation. The close association of the helical region with the C-terminal hexapeptide seems to be largely entropically driven by numerous residues forming a distinct hydrophobic cluster. The correct orientation of the ET molecule in its binding site and its subsequent biological activity may be determined at least in part by the topology of this hydrophobic cluster.

ACKNOWLEDGMENTS

We thank Dr. Peter Güntert for his help with the running of the DIANA and GLOMSA programs, Dr. David Norman for his advice on the running of X-PLOR, and Dr. James Tam for providing manuscripts prior to publication. Special thanks to Dr. Herman Schreuder for supplying a version of the SUPPOS program which was capable of handling protons and to Ken Joseph for processing some of the NOESY spectra.

Registry No. ET-3, 125692-40-2.

REFERENCES

Aumelas, A., Chiche, L., Mahe, E., Le-Nguyen, D., Sizun, P., Berthault, P., & Perly, D. (1991) *Neurochem. Int. 18*, 471–475.

Bortmann, P., Hoflack, J., Pelton, J. T., & Saudek, V. (1991) *Neurochem. Int. 18*, 491–496.

Brünger, A. T. (1990) X-PLOR *Version 2.1, User Manual*, Yale University, New Haven, CT.

Burley, S. K., & Petsko, G. A. (1988) *Adv. Protein Chem. 39*, 125–189.

Clore, G. M., & Gronenborn, A. M. (1989) *CRC Crit. Rev. Biochem. Mol. Biol. 24*, 479–564.

Clore, G. M., & Gronenborn, A. M. (1991) *Science 252*, 1390–1399.

Endo, S., Inooka, H., Ishibashi, Y., Kitada, C., Mizuta, E., & Fujino, M. (1989) *FEBS Lett. 257*, 149–154.

Ferrin, T., Huang, C. C., Jarvis, L. E., & Langridge, R. (1988) *J. Mol. Graphics 6*, 13–27.

Fleminger, G., Bousso-Mittler, D., Bdolah, A., Kloog, Y., & Sokolovsky, M. (1989) *Biochem. Biophys. Res. Commun. 162*, 1317–1323.

Galantino, M., de Castiglione, R., Tam, J. P., Liu, W., Zhang, J.-W., Cristiani, C., & Vaghi, F. (1991) *Pept.: Chem. Biol., Proc. Am. Pept. Symp., 12th*, P203.

Güntert, P., Braun, W., & Wüthrich, K. (1991) *J. Mol. Biol. 217*, 517–530.

Hendrickson, W. A. (1979) *Acta Crystallogr. 35*, 158–163.

Hirata, Y., Yoshimi, H., Emori, T., Shichiri, M., Marumo, F., Watanabe, T. X., Kumagaye, K., Nakajima, K., Kimura, T., & Sakakibara, S. (1989) *Biochem. Biophys. Res. Commun. 160*, 228–234.

Inoue, A., Yanagisawa, M., Kimura, S., Kasuya, Y., Miyauchi, T., Goto, K., & Masaki, T. (1989) *Proc. Natl. Acad. Sci. U.S.A. 86*, 2863–2867.

Kabsch, W. (1976) *Acta Crystallogr. A43*, 922–923.

Kloog, Y., & Sokolovsky, M. (1989) *Trends Pharmacol. Sci. 10*, 212–214.

Krystek, S. R., Bassolino, D. A., Novotny, J., Chen, C., Marschner, T. M., & Andersen, N. H. (1991) *FEBS Lett. 281*, 212–218.

Le Monnier de Gouville, A.-C., Lippton, H. L., Cavero, I., Summer, W. R., & Hyman, A. L. (1989) *Life Sci. 45*, 1499–1513.

MacCumber, M. W., Ross, C. A., Glaser, B. M., & Snyder, S. H. (1989) *Proc. Natl. Acad. Sci. U.S.A. 86*, 7285–7289.

Matsumoto, H., Suzuki, N., Onda, H., & Fujino, M. (1989) *Biochem. Biophys. Res. Commun. 164*, 74–80.

Mehlkopf, A. F., Korbee, D., Tiggleman, T. A., & Freeman, R. (1984) *J. Magn. Reson. 58*, 315–323.

Mills, R. G., Atkins, A. R., Harvey, T., Junius, F. K., Smith, R., & King, G. F. (1991) *FEBS Lett. 282*, 247–252.

Nakajima, K., Kumagaye, S., Nishio, H., Kuroda, H., Watanabe, T. X., Kobayashi, Y., Tamaoki, H., Kimura, T., & Sakakibara, S. (1989a) *J. Cardiovasc. Pharmacol. 13 (Suppl. 5)*, S8–S12.

Nakajima, K., Kubo, S., Kumagaye, S., Nishio, H., Tsunemi, M., Inui, T., Kuroda, H., Chino, N., Watanabe, T. X., Kimura, T., & Sakakibara, S. (1989b) *Biochem. Biophys. Res. Commun. 163*, 424–429

Nilges, M., Clore, G. M., & Gronenborn, A. M. (1988) *FEBS Lett. 239*, 129–136.

Pelton, J. T. (1991) *Neurochem. Int. 18*, 485–489.

Randall, M. D. (1991) *Pharmacol. Ther. 50*, 73–93.

Rovero, P., Patacchini, R., & Maggi, C. A. (1990) *Br. J. Pharmacol. 101*, 232–234.

Saudek, V., Hoflack, J., & Pelton, J. T. (1989) *FEBS Lett. 257*, 145–148.

Saudek, V., Hoflack, J., & Pelton, J. T. (1991) *Int. J. Pept. Protein Res. 37*, 174–179.

Vane, J. R., Bottin, R., & Masaki, T., Eds. (1989) *J. Cardiovasc. Pharmacol. 13 (Suppl. 5)*, S1–S231.

Wagner, G., Braun, W., Havel, T. F., Schaumann, T., Go, N., & Wüthrich, K. (1987) *J. Mol. Biol. 196*, 611–639.

Williamson, M. P., Havel, T. F., & Wüthrich, K. (1985) *J. Mol. Biol. 182*, 295–315.

Wüthrich, K., Billeter, M., & Braun, W. (1983) *J. Mol. Biol. 169*, 949–961.

Yanagisawa, M., & Masaki, T. (1989) *Biochem. Pharmacol. 38*, 1877–1883.